

Probing Parton Dynamics of QCD Matter with Ω and ϕ Production

L. Adamczyk,¹ J. K. Adkins,²⁰ G. Agakishiev,¹⁸ M. M. Aggarwal,³⁰ Z. Ahammed,⁴⁷ I. Alekseev,¹⁶ J. Alford,¹⁹ A. Aparin,¹⁸ D. Arkhipkin,³ E. C. Aschenauer,³ G. S. Averichev,¹⁸ V. Bairathi,²⁷ A. Banerjee,⁴⁷ R. Bellwied,⁴³ A. Bhasin,¹⁷ A. K. Bhati,³⁰ P. Bhattarai,⁴² J. Bielcik,¹⁰ J. Bielcikova,¹¹ L. C. Bland,³ I. G. Bordyuzhin,¹⁶ J. Bouchet,¹⁹ A. V. Brandin,²⁶ I. Bunzarov,¹⁸ J. Butterworth,³⁶ H. Caines,⁵¹ M. Calderón de la Barca Sánchez,⁵ J. M. Campbell,²⁸ D. Cebra,⁵ M. C. Cervantes,⁴¹ I. Chakaberia,³ P. Chaloupka,¹⁰ Z. Chang,⁴¹ S. Chattopadhyay,⁴⁷ J. H. Chen,³⁹ X. Chen,²² J. Cheng,⁴⁴ M. Cherney,⁹ W. Christie,³ G. Contin,²³ H. J. Crawford,⁴ S. Das,¹³ L. C. De Silva,⁹ R. R. Debbé,³ T. G. Dedovich,¹⁸ J. Deng,³⁸ A. A. Derevschikov,³² B. di Ruzza,³ L. Didenko,³ C. Dilks,³¹ X. Dong,²³ J. L. Drachenberg,⁴⁶ J. E. Draper,⁵ C. M. Du,²² L. E. Dunkelberger,⁶ J. C. Dunlop,³ L. G. Efimov,¹⁸ J. Engelage,⁴ G. Eppley,³⁶ R. Esha,⁶ O. Evdokimov,⁸ O. Eysler,³ R. Fatemi,²⁰ S. Fazio,³ P. Federic,¹¹ J. Fedorisin,¹⁸ Z. Feng,⁷ P. Filip,¹⁸ Y. Fisyak,³ C. E. Flores,⁵ L. Fulek,¹ C. A. Gagliardi,⁴¹ D. Garand,³³ F. Geurts,³⁶ A. Gibson,⁴⁶ M. Girard,⁴⁸ L. Greiner,²³ D. Grosnick,⁴⁶ D. S. Gunarathne,⁴⁰ Y. Guo,³⁷ A. Gupta,¹⁷ S. Gupta,¹⁷ W. Guryn,³ A. Hamad,¹⁹ A. Hamed,⁴¹ R. Haque,²⁷ J. W. Harris,⁵¹ L. He,³³ S. Heppelmann,³¹ S. Heppelmann,³ A. Hirsch,³³ G. W. Hoffmann,⁴² D. J. Hofman,⁸ S. Horvat,⁵¹ B. Huang,⁸ H. Z. Huang,⁶ X. Huang,⁴⁴ P. Huck,⁷ T. J. Humanic,²⁸ G. Igo,⁶ W. W. Jacobs,¹⁵ H. Jang,²¹ K. Jiang,³⁷ E. G. Judd,⁴ S. Kabana,¹⁹ D. Kalinkin,¹⁶ K. Kang,⁴⁴ K. Kauder,⁴⁹ H. W. Ke,³ D. Keane,¹⁹ A. Kechechyan,¹⁸ Z. H. Khan,⁸ D. P. Kikola,⁴⁸ I. Kisel,¹² A. Kisiel,⁴⁸ L. Kochenda,²⁶ D. D. Koetke,⁴⁶ T. Kollegger,¹² L. K. Kosarzewski,⁴⁸ A. F. Kraishan,⁴⁰ P. Kravtsov,²⁶ K. Krueger,² I. Kulakov,¹² L. Kumar,³⁰ R. A. Kycia,²⁹ M. A. C. Lamont,³ J. M. Landgraf,³ K. D. Landry,⁶ J. Lauret,³ A. Lebedev,³ R. Lednický,¹⁸ J. H. Lee,³ X. Li,⁴⁰ Z. M. Li,⁷ Y. Li,⁴⁴ W. Li,³⁹ X. Li,³ C. Li,³⁷ M. A. Lisa,²⁸ F. Liu,⁷ T. Ljubicic,³ W. J. Llope,⁴⁹ M. Lomnitz,¹⁹ R. S. Longacre,³ X. Luo,⁷ G. L. Ma,³⁹ R. Ma,³ Y. G. Ma,³⁹ L. Ma,³⁹ N. Magdy,⁵⁰ R. Majka,⁵¹ A. Manion,²³ S. Margetis,¹⁹ C. Markert,⁴² H. Masui,²³ H. S. Matis,²³ D. McDonald,⁴³ K. Meehan,⁵ N. G. Minaev,³² S. Mioduszewski,⁴¹ D. Mishra,²⁷ B. Mohanty,²⁷ M. M. Mondal,⁴¹ D. A. Morozov,³² M. K. Mustafa,²³ B. K. Nandi,¹⁴ Md. Nasim,⁶ T. K. Nayak,⁴⁷ G. Nigmatkulov,²⁶ L. V. Nogach,³² S. Y. Noh,²¹ J. Novak,²⁵ S. B. Nurushev,³² G. Odyniec,²³ A. Ogawa,³ K. Oh,³⁴ V. Okorokov,²⁶ D. Olivitt Jr.,⁴⁰ B. S. Page,³ R. Pak,³ Y. X. Pan,⁶ Y. Pandit,⁸ Y. Panebratsev,¹⁸ B. Pawlik,²⁹ H. Pei,⁷ C. Perkins,⁴ A. Peterson,²⁸ P. Pile,³ M. Planinic,⁵² J. Pluta,⁴⁸ N. Poljak,⁵² K. Poniatowska,⁴⁸ J. Porter,²³ M. Posik,⁴⁰ A. M. Poskanzer,²³ J. Putschke,⁴⁹ H. Qiu,²³ A. Quintero,¹⁹ S. Ramachandran,²⁰ R. Raniwala,³⁵ S. Raniwala,³⁵ R. L. Ray,⁴² H. G. Ritter,²³ J. B. Roberts,³⁶ O. V. Rogachevskiy,¹⁸ J. L. Romero,⁵ A. Roy,⁴⁷ L. Ruan,³ J. Rusnak,¹¹ O. Rusnakova,¹⁰ N. R. Sahoo,⁴¹ P. K. Sahu,¹³ I. Sakrejda,²³ S. Salur,²³ J. Sandweiss,⁵¹ A. Sarkar,¹⁴ J. Schambach,⁴² R. P. Scharenberg,³³ A. M. Schmah,²³ W. B. Schmidke,³ N. Schmitz,²⁴ J. Seger,⁹ P. Seyboth,²⁴ N. Shah,³⁹ E. Shahaiev,¹⁸ P. V. Shanmuganathan,¹⁹ M. Shao,³⁷ M. K. Sharma,¹⁷ B. Sharma,³⁰ W. Q. Shen,³⁹ S. S. Shi,⁷ Q. Y. Shou,³⁹ E. P. Sichtermann,²³ R. Sikora,¹ M. Simko,¹¹ M. J. Skoby,¹⁵ N. Smirnov,⁵¹ D. Smirnov,³ L. Song,⁴³ P. Sorensen,³ H. M. Spinka,² B. Srivastava,³³ T. D. S. Stanislaus,⁴⁶ M. Stepanov,³³ R. Stock,¹² M. Strikhanov,²⁶ B. Stringfellow,³³ M. Sumner,¹¹ B. Summa,³¹ Z. Sun,²² X. M. Sun,⁷ Y. Sun,³⁷ X. Sun,²³ B. Surrow,⁴⁰ N. Svirida,¹⁶ M. A. Szelezniak,²³ Z. Tang,³⁷ A. H. Tang,³ T. Tarnowsky,²⁵ A. Tawfik,⁵⁰ J. H. Thomas,²³ A. R. Timmins,⁴³ D. Tlusty,¹¹ M. Tokarev,¹⁸ S. Trentalange,⁶ R. E. Tribble,⁴¹ P. Tribedy,⁴⁷ S. K. Tripathy,¹³ B. A. Trzeciak,¹⁰ O. D. Tsai,⁶ T. Ullrich,³ D. G. Underwood,² I. Upsal,²⁸ G. Van Buren,³ G. van Nieuwenhuizen,³ M. Vandenbroucke,⁴⁰ R. Varma,¹⁴ A. N. Vasiliev,³² R. Vertesi,¹¹ F. Videbæk,³ Y. P. Viyogi,⁴⁷ S. Vokal,¹⁸ S. A. Voloshin,⁴⁹ A. Vossen,¹⁵ G. Wang,⁶ H. Wang,³ J. S. Wang,²² Y. Wang,⁷ Y. Wang,⁴⁴ F. Wang,³³ J. C. Webb,³ G. Webb,³ L. Wen,⁶ G. D. Westfall,²⁵ H. Wieman,²³ S. W. Wissink,¹⁵ R. Witt,⁴⁵ Y. F. Wu,⁷ Z. G. Xiao,⁴⁴ W. Xie,³³ K. Xin,³⁶ Y. F. Xu,³⁹ Q. H. Xu,³⁸ H. Xu,²² N. Xu,²³ Z. Xu,³ Y. Yang,²² C. Yang,³⁷ S. Yang,³⁷ Y. Yang,⁷ Q. Yang,³⁷ Z. Ye,⁸ P. Yepes,³⁶ L. Yi,⁵¹ K. Yip,³ I. -K. Yoo,³⁴ N. Yu,⁷ H. Zbroszczyk,⁴⁸ W. Zha,³⁷ J. B. Zhang,⁷ Z. Zhang,³⁹ J. Zhang,³⁸ S. Zhang,³⁹ X. P. Zhang,⁴⁴ J. Zhang,²² Y. Zhang,³⁷ F. Zhao,⁶ J. Zhao,⁷ C. Zhong,³⁹ L. Zhou,³⁷ X. Zhu,⁴⁴ Y. Zoulkarneeva,¹⁸ and M. Zyzak¹²

(STAR Collaboration)

¹AGH University of Science and Technology, Cracow 30-059, Poland

²Argonne National Laboratory, Argonne, Illinois 60439, USA

³Brookhaven National Laboratory, Upton, New York 11973, USA

⁴University of California, Berkeley, California 94720, USA

⁵University of California, Davis, California 95616, USA

⁶University of California, Los Angeles, California 90095, USA

⁷Central China Normal University (HZNU), Wuhan 430079, China

⁸University of Illinois at Chicago, Chicago, Illinois 60607, USA

⁹Creighton University, Omaha, Nebraska 68178, USA

- ¹⁰Czech Technical University in Prague, FNSPE, Prague, 115 19, Czech Republic
¹¹Nuclear Physics Institute AS CR, 250 68 Řež/Prague, Czech Republic
¹²Frankfurt Institute for Advanced Studies FIAS, Frankfurt 60438, Germany
¹³Institute of Physics, Bhubaneswar 751005, India
¹⁴Indian Institute of Technology, Mumbai 400076, India
¹⁵Indiana University, Bloomington, Indiana 47408, USA
¹⁶Alkhanov Institute for Theoretical and Experimental Physics, Moscow 117218, Russia
¹⁷University of Jammu, Jammu 180001, India
¹⁸Joint Institute for Nuclear Research, Dubna, 141 980, Russia
¹⁹Kent State University, Kent, Ohio 44242, USA
²⁰University of Kentucky, Lexington, Kentucky, 40506-0055, USA
²¹Korea Institute of Science and Technology Information, Daejeon 305-701, Korea
²²Institute of Modern Physics, Lanzhou 730000, China
²³Lawrence Berkeley National Laboratory, Berkeley, California 94720, USA
²⁴Max-Planck-Institut für Physik, Munich 80805, Germany
²⁵Michigan State University, East Lansing, Michigan 48824, USA
²⁶Moscow Engineering Physics Institute, Moscow 115409, Russia
²⁷National Institute of Science Education and Research, Bhubaneswar 751005, India
²⁸Ohio State University, Columbus, Ohio 43210, USA
²⁹Institute of Nuclear Physics PAN, Cracow 31-342, Poland
³⁰Panjab University, Chandigarh 160014, India
³¹Pennsylvania State University, University Park, Pennsylvania 16802, USA
³²Institute of High Energy Physics, Protvino 142281, Russia
³³Purdue University, West Lafayette, Indiana 47907, USA
³⁴Pusan National University, Pusan 609735, Republic of Korea
³⁵University of Rajasthan, Jaipur 302004, India
³⁶Rice University, Houston, Texas 77251, USA
³⁷University of Science and Technology of China, Hefei 230026, China
³⁸Shandong University, Jinan, Shandong 250100, China
³⁹Shanghai Institute of Applied Physics, Shanghai 201800, China
⁴⁰Temple University, Philadelphia, Pennsylvania 19122, USA
⁴¹Texas A&M University, College Station, Texas 77843, USA
⁴²University of Texas, Austin, Texas 78712, USA
⁴³University of Houston, Houston, Texas 77204, USA
⁴⁴Tsinghua University, Beijing 100084, China
⁴⁵United States Naval Academy, Annapolis, Maryland, 21402, USA
⁴⁶Valparaiso University, Valparaiso, Indiana 46383, USA
⁴⁷Variable Energy Cyclotron Centre, Kolkata 700064, India
⁴⁸Warsaw University of Technology, Warsaw 00-661, Poland
⁴⁹Wayne State University, Detroit, Michigan 48201, USA
⁵⁰World Laboratory for Cosmology and Particle Physics (WLCAPP), Cairo 11571, Egypt
⁵¹Yale University, New Haven, Connecticut 06520, USA
⁵²University of Zagreb, Zagreb, HR-10002, Croatia

We present measurements of Ω and ϕ production at mid-rapidity from Au+Au collisions at nucleon-nucleon center-of-mass energies $\sqrt{s_{\text{NN}}} = 7.7, 11.5, 19.6, 27$ and 39 GeV by the STAR experiment at the Relativistic Heavy Ion Collider (RHIC). Motivated by the coalescence formation mechanism for these strange hadrons, we study the ratios of $N(\Omega^- + \bar{\Omega}^+)/ (2N(\phi))$. These ratios as a function of transverse momentum (p_T) fall on a consistent trend at high collision energies, but start to show deviations in peripheral collisions at $\sqrt{s_{\text{NN}}} = 19.6, 27$ and 39 GeV, and in central collisions at 11.5 GeV in the intermediate p_T region of 2.4 – 3.6 GeV/ c . We further evaluate empirically the strange quark p_T distributions at hadronization by studying the Ω/ϕ ratios scaled by the number of constituent quarks. The NCQ-scaled Ω/ϕ ratios show a suppression of strange quark production in central collisions at 11.5 GeV compared to $\sqrt{s_{\text{NN}}} \geq 19.6$ GeV. The shapes of the presumably thermal strange quark distributions in 0-60% most central collisions at 7.7 GeV show significant deviations from those in 0-10% most central collisions at higher energies. These features suggest that there is likely a change of the underlying strange quark dynamics in the transition from quark-matter to hadronic matter at collision energies below 19.6 GeV.

PACS numbers: 25.75.Dw, 25.75.Nq

Lattice quantum chromodynamics (QCD) calculations suggest that, at high temperature and low baryon chem-

ical potential (μ_B), the transition from the Quark Gluon Plasma (QGP) to the state of a hadron gas is smooth

and continuous (cross-over transition) [1]. At lower temperatures and high μ_B , theoretical calculations predict a first order phase transition [2] which may end at a critical point [3]. The mapping of the QCD phase diagram has been a subject of intensive theoretical and experimental activities in the past decades. In central Pb-Pb collisions at Super Proton Synchrotron (SPS), the enhanced production of Ω at $\sqrt{s_{NN}} = 8.8$ and 17.3 GeV [4–7] and ϕ mesons at $\sqrt{s_{NN}} = 6.3$ –17.3 GeV [8] compared to π mesons has been considered as a QGP signal [9]. Multi-strange hadrons such as $\Omega(sss)$ hyperons and $\phi(s\bar{s})$ mesons are important probes for the search of the QCD phase boundaries [10, 11]. The Ω hyperons and ϕ mesons are expected to have relatively small hadronic interaction cross sections [12, 13]. Therefore, they can carry the information directly from the chemical freeze-out stage with little or no distortion due to hadronic rescattering. In addition, the measured Ω and ϕ yields suffer minimal distortion from decay feed-down. As a result, the production of the Ω and ϕ particles offers a unique advantage in probing the transition from partonic to hadronic dynamics.

In heavy ion collisions at the top RHIC energy of $\sqrt{s_{NN}} = 200$ GeV, model calculations [14–18] and experimental data suggest that particles at intermediate p_T are formed via the coalescence of low p_T quarks from the bulk partonic matter and/or fragmented hard partons. Experimentally, baryon to meson ratios have been found to be large compared to those from elementary collisions [10, 19–22]. The measured elliptic flow v_2 has been found to scale with the number of constituent quarks (NCQ) for both baryons and mesons [23] in Au+Au collisions at the top RHIC energy. In order to explain these observations, coalescence model calculations require the development of collectivity among constituent quarks during the partonic phase. This partonic collectivity has been considered as an important evidence for the formation of deconfined QCD matter with partonic degrees of freedom in Au+Au collisions at the highest RHIC energy [10, 19–22].

In order to map out the phase diagram of the QCD matter, a Beam Energy Scan (BES) program has been initiated at RHIC with Au+Au collisions at $\sqrt{s_{NN}} = 7.7$ –39 GeV [24]. These collisions allow us to reach a broad range of temperature and μ_B in the QCD phase diagram [25] and search for a possible beam energy region where the underlying dynamics are different from those of partonic matter observed in Au+Au collisions at the top RHIC energy.

The STAR experiment, which has a large acceptance detector system [26], has collected Au+Au collision data at $\sqrt{s_{NN}} = 7.7$, 11.5 and 39 GeV in 2010, and at $\sqrt{s_{NN}} = 19.6$ and 27 GeV in 2011. Compared to previous measurements at SPS [4–8], RHIC offers wide range of beam energies. In addition, the STAR detector provides uniform acceptance over different energies and extensive reach to the intermediate p_T range for both Ω and ϕ mesons for different centralities. In this letter,

we present the first STAR measurements of mid-rapidity ($|y| < 0.5$) Ω and ϕ production with a broad p_T coverage for various collision centrality bins at selected energies for the BES. With guidance from coalescence formation mechanism for primordial particles such as Ω and ϕ , we examine features in particle production and explore possible changes from bulk partonic coalescence to hadron dominated dynamics as the colliding energy decreases.

A minimum bias trigger was used to record Au+Au collision events in this analysis. The trigger was defined using a coincidence of signals from either the Zero Degree Calorimeters, Vertex Position Detectors or Beam-Beam Counters [27, 28]. STAR’s Time Projection Chamber (TPC) [29] was used for tracking of charged particles and particle identification. In the offline data analysis, we require the radial position of the reconstructed primary vertex to be within 2 cm of the beam axis to suppress events from collisions with the beam pipe (radius of 3.95 cm). To ensure nearly uniform detector acceptance, the analyzed events were required to have a primary Z vertex (along beam direction) within ± 70 cm from the center of the TPC for $\sqrt{s_{NN}} = 7.7$, 19.6, and 27 GeV collisions and ± 50 cm, ± 40 cm for $\sqrt{s_{NN}} = 11.5$ and 39 GeV, respectively. After the event selection, we obtain approximately 4, 12, 36, 70 and 130 million Au+Au minimum bias triggered events at $\sqrt{s_{NN}} = 7.7$, 11.5, 19.6, 27 and 39 GeV, respectively. The collision centrality was determined by comparing the uncorrected charged hadron multiplicity measured from the TPC at mid-rapidity ($|\eta| < 0.5$) with Monte Carlo Glauber simulations [27, 28].

The multi-strange hadron signals and raw yields were obtained from the invariant mass distributions reconstructed through their hadronic decay channels: $\phi \rightarrow K^+ + K^-$ and $\Omega^-(\bar{\Omega}^+) \rightarrow \Lambda(\bar{\Lambda}) + K^-(K^+)$. The decay daughters $\Lambda(\bar{\Lambda})$ were reconstructed through $\Lambda(\bar{\Lambda}) \rightarrow p(\bar{p}) + \pi^-(\pi^+)$. Charged hadrons ($\pi^\pm, K^\pm, p, \bar{p}$) were identified by their specific energy loss (dE/dx) in the TPC gas [29]. The combinatorial background of the weakly decaying particles $\Lambda(\bar{\Lambda})$ and $\Omega^-(\bar{\Omega}^+)$ was reduced by geometrical cuts on their decay topology [28, 30]. The $\Omega^-(\bar{\Omega}^+)$ combinatorial background was estimated by rotating $K^-(K^+)$ tracks at 5 different angles from $\pi/3$ to $5\pi/3$ and normalizing the invariant mass distribution to the mass window of (1.625 GeV/ c^2 , 1.655 GeV/ c^2) and (1.69 GeV/ c^2 , 1.72 GeV/ c^2). The $\Omega^-(\bar{\Omega}^+)$ raw yields were extracted by counting the signals within a mass window from 1.660 to 1.685 GeV/ c^2 after subtracting the rotational background. The K^+K^- combinatorial background in ϕ meson reconstruction was subtracted with the mixed event technique [10, 31]. The ϕ meson raw yields were determined by a Breit-Wigner + polynomial function (up to second order) fit to the mixed-event-background-subtracted K^+K^- invariant mass distribution [10, 31].

Figures 1 and 2 show the p_T spectra of ϕ , and $\Omega^-(\bar{\Omega}^+)$ at mid-rapidity ($|y| < 0.5$) for different centralities from Au+Au collisions at $\sqrt{s_{NN}} = 7.7$ –39 GeV. The spec-

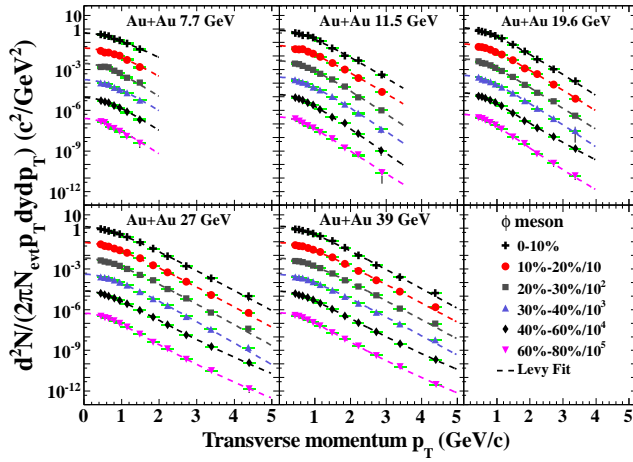


FIG. 1: (Color online) Mid-rapidity ($|y| < 0.5$) ϕ meson p_T spectra from Au+Au collisions at different centralities and energies ($\sqrt{s_{NN}} = 7.7 - 39$ GeV). The green bands represent systematic errors. The dashed curves represent fits to the experimental data with a Levy function [10].

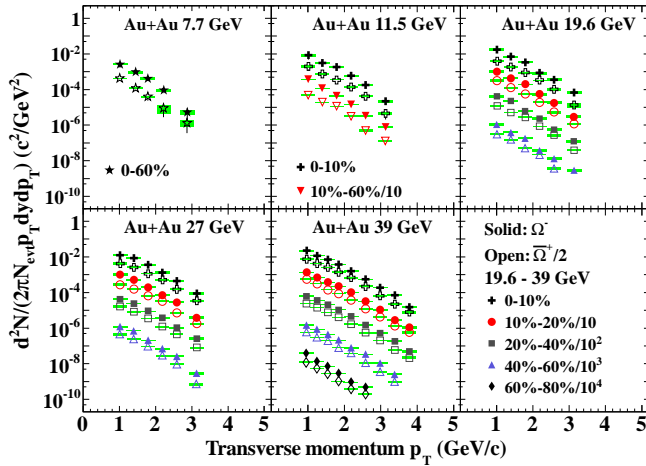


FIG. 2: (Color online) Mid-rapidity ($|y| < 0.5$) Ω^- (Ω^+) p_T spectra from Au+Au collisions at different centralities and energies ($\sqrt{s_{NN}} = 7.7 - 39$ GeV). The open symbols represent Ω^+ and solid symbols represent Ω^- . The green bands denote systematic errors.

tra were corrected for reconstruction efficiency and geometrical acceptance. The systematic errors mainly come from two sources: the different signal extraction techniques, and the reconstruction efficiency corrections. They were studied as a function of p_T and were obtained by exploring the dependence of invariant yields on various raw yield extraction techniques including different fit/counting ranges and different fit functions, and on different combinations of analysis cuts. For the ϕ meson, relative systematic errors of invariant yields vary from 10%-16% at $\sqrt{s_{NN}} = 11.5 - 39$ GeV to 17%-21% at $\sqrt{s_{NN}} = 7.7$ GeV. The systematic errors in 0-10% central collisions are generally larger than those in 60%-80% pe-

ripheral collisions by 2%-3% due to greater combinatorial backgrounds. For $p_T < 0.8$ GeV/c in central collisions, the uncertainty of ϕ meson raw yield extraction is dominant. However, for $p_T > 1.6$ GeV/c the main source of systematic error is the differences in track selection cuts. For the Ω invariant yields, the relative systematic errors vary from $\sim 5\%$ to 20%, and are dominated by the signal extraction methods. Due to the higher combinatorial background in $p_T \lesssim 1.2$ GeV/c and low statistics at $p_T \gtrsim 2.8$ GeV/c, the systematic errors are found to be larger in the corresponding p_T windows. The systematic uncertainties have a weak centrality dependence and their energy dependences for Ω and ϕ particles are similar. The systematic errors of invariant yields of ϕ and Ω are shown as green bands in Figs. 1 and 2 for each p_T bin.

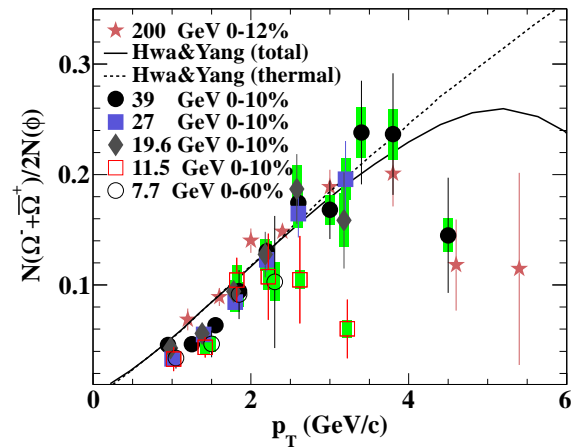


FIG. 3: (Color online) The baryon-to-meson ratio, $N(\Omega^- + \Omega^+)/2N(\phi)$, as a function of p_T in mid-rapidity ($|y| < 0.5$) from Au+Au collisions at $\sqrt{s_{NN}} = 7.7 - 200$ GeV. The green bands denote systematic errors. The solid and dashed lines represent recombination model calculations for central collisions at $\sqrt{s_{NN}} = 200$ GeV [15] with total and thermal strange quark contributions, respectively.

We present baryon-to-meson ratios, $N(\Omega^- + \Omega^+)/2N(\phi)$, as a function of p_T from Au+Au collisions for various beam energies from $\sqrt{s_{NN}} = 7.7$ to 200 GeV in Fig. 3 and for various collision centralities in Fig. 4, respectively. Data from 200 GeV Au+Au collisions are from previously published STAR results [10]. Coalescence or recombination models [15–17] have been used to describe particle productions in nucleus-nucleus collisions at RHIC. In particular, a model calculation by Hwa and Yang for Au+Au collisions at $\sqrt{s_{NN}} = 200$ GeV [15] predicted that most of the Ω and ϕ yields up to the intermediate p_T region are from coalescence/recombination of thermal strange quarks. The straight dotted line assumed that these thermal strange quarks have exponential p_T distributions. Deviations from the straight line at high p_T were attributed to recombination with strange quarks from high p_T showers. Deviations from the theory calculation at low

p_T could indicate that thermal strange quarks may not have an exponential distribution. Possibly, other particle production dynamics may also contribute deviations from coalescence model calculations.

In Fig. 3 the measured $N(\Omega^- + \bar{\Omega}^+)/2N(\phi)$ ratios from central Au+Au collisions at $\sqrt{s_{\text{NN}}} = 19.6, 27$ and 39 GeV follow closely the ratio from 200 GeV and are consistent with a picture of coalescence/recombination dynamics over a broad p_T range of 1–4 GeV/c. The ratios at 11.5 GeV seem to deviate from the trend observed at higher beam energies. In particular, the ratios at 11.5 GeV appear to turn down around p_T of 2 GeV/c while those at higher beam energies such as 39 and 200 GeV peak at p_T of 3 GeV/c or above. The collision centrality dependence of the $N(\Omega^- + \bar{\Omega}^+)/2N(\phi)$ ratios in Fig. 4(a)-(d) shows distinct differences between the 40%–60% centrality bin and the other centrality bins for Au+Au collisions at 19.6 and 27 GeV. Furthermore, the ratios from the peripheral collisions of 40%–60% at 27 GeV are similar in magnitude to the ratios from collisions at 11.5 GeV. Because the Ω and ϕ particles have small hadronic rescattering cross sections [32], the change in these ratios is likely to originate from the partonic phase. The decrease in the $N(\Omega^- + \bar{\Omega}^+)/2N(\phi)$ ratios from central collisions at 11.5 GeV compared to those at 19.6 GeV or above may indicate a significant change in the hadron formation dynamics and/or in strange quark p_T distributions at the lower energy. Such a change may arise from a transition from hadronic to partonic dynamics with increasing beam energy. The turn-over in the ratios from Au+Au collisions below 11.5 GeV beam energy is unlikely due to contributions of high p_T shower partons as suggested by model calculation from Hwa and Yang [15] because of relatively low p_T particles involved.

We illustrate qualitatively the change in the underlying bulk strange quark p_T distribution by following the procedure developed in Ref. [18]. We assume that the Ω baryons are formed from coalescence of three strange quarks of approximately equal momentum and the ϕ mesons from two strange quarks. In the coalescence framework, the Ω baryon production probability is proportional to the local strange quark density, $f_s^3(p_T^s)$, and the ϕ meson is proportional to $f_s(p_T^s)f_{\bar{s}}(p_T^{\bar{s}})$, where f_s ($f_{\bar{s}}$) is the strange (anti-strange) quark p_T distribution at hadronization. Assuming that strange quarks and anti-strange quarks have a similar slope of p_T distribution, the NCQ-scaled ratio $\frac{N(\Omega^- + \bar{\Omega}^+) |_{p_T^{\Omega} = 3p_T^{\phi}}}{2N(\phi) |_{p_T^{\phi} = 2p_T^{\bar{s}}}}$ could reflect the strange quark distribution at hadronization. We note that theoretical calculations with a more sophisticated recombination scheme have been developed by He *et al.* [33] and the extracted strange quark distribution is similar to that from the present approach.

Figure 5(a) shows the NCQ-scaled $\frac{N(\Omega^- + \bar{\Omega}^+) |_{p_T^{\Omega} = 3p_T^{\phi}}}{2N(\phi) |_{p_T^{\phi} = 2p_T^{\bar{s}}}}$ ratios as a function of $p_T^s = p_T/n_q$ at mid-rapidity ($|y| < 0.5$) from central Au+Au collisions at $\sqrt{s_{\text{NN}}} =$

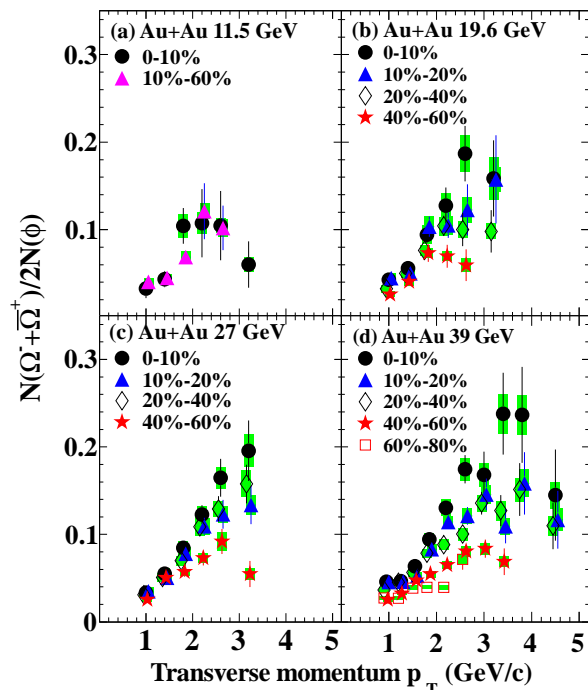


FIG. 4: (Color online) Centrality dependence of $N(\Omega^- + \bar{\Omega}^+)/2N(\phi)$ ratios, as a function of p_T in mid-rapidity ($|y| < 0.5$) from Au+Au collisions at $\sqrt{s_{\text{NN}}} = 11.5, 19.6, 27$ and 39 GeV. The green bands denote systematical errors.

11.5 – 200 GeV as well as 0-60% collisions at 7.7 GeV. Here $N(\Omega^- + \bar{\Omega}^+)$ and $N(\phi)$ denote invariant yields of $(\Omega^- + \bar{\Omega}^+)$ and ϕ , respectively. Since the p_T bin widths used for the Ω^- ($\bar{\Omega}^+$) and ϕ meson spectra do not match, we use our Levy fit (see Fig. 1) to interpolate the invariant yield of ϕ meson at desired p_T . The NCQ-scaled $\frac{N(\Omega^- + \bar{\Omega}^+) |_{p_T^{\Omega} = 3p_T^{\phi}}}{2N(\phi) |_{p_T^{\phi} = 2p_T^{\bar{s}}}}$ ratios at all energies can be fit with a Boltzmann distribution $\frac{q_s A m_T}{T(m_s + T)} e^{-(m_T - m_s)/T}$, where m_s is the effective strange quark mass of 0.46 GeV/c² from Ref. [16], m_T is the transverse mass ($\sqrt{m_s^2 + p_T^2}$), T is the slope parameter of the exponential function which may be related to the freeze-out temperature and radial expansion velocity of strange quarks [30]. Considering different yields ratios of \bar{s} quark over s quark with collision energies, that is, $f_s(p_T^s) = r(\sqrt{s_{\text{NN}}})f_{\bar{s}}(p_T^{\bar{s}})$, where $r^3(\sqrt{s_{\text{NN}}}) = \frac{dN}{dy}(\bar{\Omega}^+)/\frac{dN}{dy}(\Omega^-)$, we include a correction factor $g_s = (1+r^3)/r$ in the Boltzmann distribution function (based on the coalescence calculation [15]), and then A is proportional to strange quark rapidity density.

The fitting parameters A and T , and 1σ contours are shown in Fig. 5(b). Figs. 5(a)-(b) show that the derived strange quark distributions vary little in shape as a function of beam energy from 11.5 GeV to 200 GeV. The amplitude parameter A at 11.5 GeV, however, seems to be noticeably smaller than those data of 19.6 GeV or above. Based on coalescence model [15], the smaller

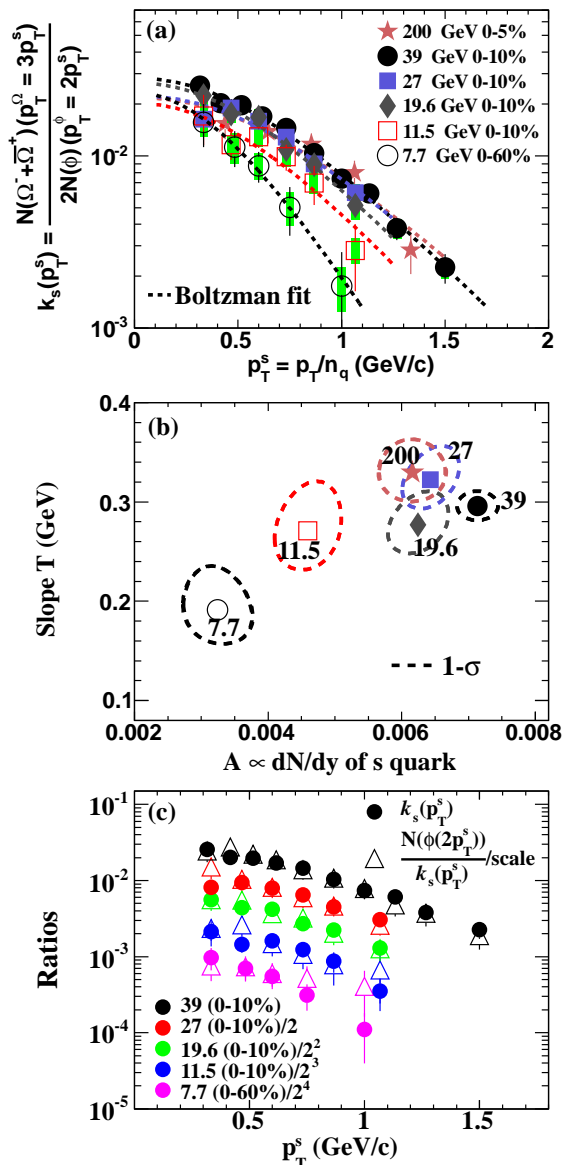


FIG. 5: (Color online) (a) NCQ-scaled $N(\Omega^- + \bar{\Omega}^+)/2N(\phi)$ ratios, as a function of p_T/n_q in mid-rapidity ($|y| < 0.5$) from Au+Au collisions at $\sqrt{s_{NN}} = 7.7 - 200$ GeV. Here n_q is the number of constituent quarks of each hadron. The green bands denote systematic errors. Dashed lines are Boltzmann fits to data. (b) The fitting parameters A and T , and 1σ contours (including statistic and systematic errors). (c) The ratios of $f_s(p_T^s)$ and scaled $\frac{N(\phi(2p_T^s))}{f_s(p_T^s)}$ as a function of p_T^s . The scale factors are 394.4, 763.7, 742.8, 870.9, and 746.5 for $\sqrt{s_{NN}} = 7.7, 11.5, 19.6, 27,$ and 39 GeV, respectively.

strange quark local density at 11.5 GeV is probably responsible for the smaller $N(\Omega^- + \bar{\Omega}^+)/2N(\phi)$ ratios as shown in Fig. 3, where the first two low p_T points at 11.5 GeV are systematically lower than those at $\sqrt{s_{NN}} \geq 19.6$ GeV. At 7.7 GeV, the slope parameter T is smaller than those data of 19.6 GeV or above, with a 1.8σ standard deviation from the 19.6 GeV result. We note that one

possible reason for the deviation of T is the centrality difference since the data at 7.7 GeV are for 0-60% while those at other energies are for central collisions. In the framework of the coalescence mechanism, our derived ratio distribution can be sensitive to both the local density and the p_T distribution of strange quarks. Our data of 19.6 GeV or above show little beam energy dependence suggesting strange quark equilibration may have been approximately achieved in those central collisions, possibly due to strange quark dynamics rather than hadronic processes [34]. The variation of the 11.5 GeV data may arise from the strangeness non-equilibration and the presence of a strangeness phase space suppression factor ($\gamma_s < 1$) [30]. A possible transition in the collision dynamics and in the dominate degrees of freedom (partonic versus hadronic) below 19.6 GeV needs further experimental investigation with more experimental probes and with larger data samples [35].

Recently, the ALICE experiment reported an observation of nearly flat ratios of proton to ϕ as a function of p_T in central Pb+Pb collisions at $\sqrt{s_{NN}} = 2.76$ TeV [36]. It was argued that the similarity in shapes of the p_T spectra indicates that the radial flow of these particles is mostly determined by the masses of these particles as hydrodynamical calculations predicted, instead of by the number of constituent quarks as expected from coalescence models [36]. The ALICE proton to ϕ ratios as a function of p_T also showed a very strong dependence on collision centrality. We note that such a strong dependence is an indication that the protons undergo considerable rescattering during the hadronic evolution as expected from the hybrid model calculation [32]. It is important to disentangle the hadronic rescattering contributions to the radial flow for ordinary hadrons in order to address the partonic flow prior to hadronization. We have used the Ω and ϕ spectra to carry out another independent check on the coalescence picture: we can obtain the strange quark p_T distribution from the quark number scaled Ω to ϕ ratios as in Fig. 5(a); and we can calculate another strange quark p_T distribution by dividing the ϕ with the previously obtained strange quark distribution. Fig. 5(c) shows these two strange quark distributions. The consistency of these distributions indicates that there is one unique strange quark distribution which can explain both Ω and ϕ p_T spectra, a necessary condition for coalescence model.

In summary, STAR has measured the production of multi-strange hadrons Ω and ϕ at mid-rapidity from Au+Au collisions at $\sqrt{s_{NN}} = 7.7, 11.5, 19.6, 27$ and 39 GeV from the BES program at RHIC. The $N(\Omega^- + \bar{\Omega}^+)/2N(\phi)$ ratios at intermediate p_T in peripheral collisions are found to be lower than those in central collisions at 19.6, 27 and 39 GeV. The ratios from 11.5 GeV central collisions are systematically lower than those from collisions at 19.6 GeV or above for $p_T > 2.4$ GeV/c. The NCQ-scaled Ω/ϕ ratios show a suppression of strange quark production in 11.5 GeV compared to $\sqrt{s_{NN}} \geq 19.6$ GeV. The shapes of the presumably thermal strange

quark distributions in 0-60% most central collisions at 7.7 GeV show significant deviations from those in 0-10% most central collisions at higher energies. These features suggest that there is likely a change in the underlying strange quark dynamics in the bulk QCD matter responsible for Ω and ϕ production. Our measurements point to collision energies below 19.6 GeV for further investigation of a possible transition from partonic dominant matter ($\sqrt{s_{NN}} > 19.6$ GeV) to hadronic dominant matter ($\sqrt{s_{NN}} < 11.5$ GeV).

We thank the RHIC Operations Group and RCF at BNL, the NERSC Center at LBNL, the KISTI Center in Korea, and the Open Science Grid consortium for

providing resources and support. This work was supported in part by the Office of Nuclear Physics within the U.S. DOE Office of Science, the U.S. NSF, the Ministry of Education and Science of the Russian Federation, NNSFC, CAS, MoST (973 Program No. 2014CB845400) and MoE of China, the Korean Research Foundation, GA and MSMT of the Czech Republic, FIAS of Germany, DAE, DST, and UGC of India, the National Science Centre of Poland, National Research Foundation, the Ministry of Science, Education and Sports of the Republic of Croatia, and RosAtom of Russia. We thank Rudolph C. Hwa for valuable discussions.

-
- [1] Y. Aoki *et al.*, Nature **443**, 675 (2006).
 [2] S. Ejiri, Phys. Rev. D **78**, 074507 (2008); E. S. Bowman and J. I. Kapusta, Phys. Rev. C **79**, 015202 (2009).
 [3] M. A. Stephanov, Prog. Theor. Phys. Suppl. **153**, 139 (2004); Z. Fodor and S. D. Katz, JHEP **0404**, 50 (2004); R. V. Gavai and S. Gupta, Phys. Rev. D **78**, 114503 (2008).
 [4] C. Blume for the NA49 Collaboration, Proceedings to the ISMD09 Conference, arXiv:0910.5815 [nucl-ex].
 [5] C. Alt *et al.* (NA49 Collaboration), Phys. Rev. Lett. **94**, 192301 (2005).
 [6] D. Elia for the NA57 Collaboration, J. Phys. G: Nucl. Part. Phys. **31**, S135 (2005).
 [7] F. Antinori *et al.* (NA57 Collaboration), J. Phys. G: Nucl. Part. Phys. **31**, 1345 (2006).
 [8] C. Alt *et al.* (NA49 Collaboration), Phys. Rev. C **78**, 044907 (2008).
 [9] J. Rafelski, B. Müller, Phys. Rev. Lett. **48**, 1066 (1982).
 [10] B. I. Abelev *et al.* (STAR Collaboration), Phys. Rev. Lett. **99**, 112301 (2007); Phys. Rev. C **79**, 064903 (2009).
 [11] B. Mohanty, N. Xu, J. Phys. G **36**, 064022 (2009); K. J. Wu, F. Liu, and N. Xu, J. Phys. G **37**, 094029 (2010); J. Tian *et al.*, Phys. Rev. C **79**, 067901 (2009); Md. Nasim, B. Mohanty, and N. Xu, Phys. Rev. C **87**, 014903 (2013).
 [12] H. van Hecke, H. Sorge, and N. Xu, Phys. Rev. Lett. **81**, 5764 (1998).
 [13] A. Shor, Phys. Rev. Lett. **54**, 1122 (1985).
 [14] D. Molnár and S. A. Voloshin, Phys. Rev. Lett. **91**, 092301 (2003).
 [15] R. C. Hwa and C. B. Yang, Phys. Rev. C **66**, 025205 (2002); Phys. Rev. C **75**, 054904 (2007).
 [16] R. J. Fries, B. Müller, C. Nonaka, and S. A. Bass, Phys. Rev. Lett. **90**, 202303 (2003); Phys. Rev. C **68**, 044902 (2003).
 [17] V. Greco, C. M. Ko, and P. Lévai, Phys. Rev. Lett. **90**, 202302 (2003); Phys. Rev. C **68**, 034904 (2003).
 [18] J. H. Chen *et al.*, Phys. Rev. C **78**, 034907 (2008).
 [19] K. Adcox *et al.* (PHENIX Collaboration), Phys. Rev. C **69**, 024904 (2004).
 [20] B. I. Abelev *et al.* (STAR Collaboration), Phys. Rev. Lett. **97**, 152301 (2006); Phys. Lett. B **655**, 104 (2007).
 [21] G. Agakishiev *et al.* (STAR Collaboration), Phys. Rev. Lett. **108**, 072301 (2012).
 [22] B. Abelev *et al.* (ALICE Collaboration), Phys. Rev. Lett. **111**, 222301 (2013).
 [23] J. Adams *et al.* (STAR Collaboration), Phys. Rev. Lett. **92**, 052302 (2004).
 [24] M. M. Aggarwal *et al.* (STAR Collaboration), arXiv:1007.2613.
 [25] J. Cleymans *et al.*, Phys. Rev. C **73**, 034905 (2006); F. Becattini, J. Manninen and M. Gaździcki, Phys. Rev. C **73**, 044905 (2006); A. Andronic, P. Braun-Munzinger and J. Stachel, Nucl. Phys. A **772**, 167 (2006).
 [26] K. H. Ackermann *et al.* (STAR Collaboration), Nucl. Instrum. Meth. A **499**, 624 (2003).
 [27] L. Adamczyk *et al.* (STAR Collaboration), Phys. Rev. C **86**, 054908 (2012).
 [28] L. Adamczyk *et al.* (STAR Collaboration), Phys. Rev. C **88**, 014902 (2013).
 [29] K. H. Ackermann *et al.* (STAR Collaboration), Nucl. Instrum. Meth. A **499**, 624 (2003).
 [30] J. Adams *et al.* (STAR Collaboration), Phys. Rev. Lett. **92**, 182301 (2004); Phys. Rev. Lett. **98**, 062301 (2008).
 [31] J. Adams *et al.* (STAR Collaboration), Phys. Lett. B **612**, 181 (2005); B. I. Abelev *et al.* (STAR Collaboration), Phys. Lett. B **673**, 183 (2009).
 [32] T. Hirano *et al.*, Phys. Rev. C **77**, 044909 (2008).
 [33] M. He, R. J. Fries, and R. Rapp, Phys. Rev. C **82**, 034907 (2010).
 [34] P. Koch, B. Müller, and J. Rafelski, Phys. Rep. **142**, 167 (1986).
 [35] L. Adamczyk *et al.* (STAR Collaboration), Phys. Rev. Lett. **110**, 142301 (2013).
 [36] B. Abelev *et al.* (ALICE Collaboration), Phys. Rev. C **91**, 024609 (2015).